Edinburgh Research Explorer

Suspended MoTe2 field effect transistors with ionic liquid gate

Suspended MoTe$_2$ Field Effect Transistors with Ionic Liquid Gate

W. R. Choi[1], J. H. Hong[1], Y. G. You[1], E. E. B. Campbell[1,2] and S. H. Jhang[1, a)]

[1] *School of Physics, Konkuk University, Seoul 05029, Korea*

[2] *EaStCHEM, School of Chemistry, Edinburgh University, David Brewster Road, Edinburgh EH9 3FJ, United Kingdom*

The electrical performance of suspended few-layer MoTe$_2$ field-effect-transistors with ionic liquid gating has been investigated. The suspended structure not only enhances the mobility of MoTe$_2$ by removing the influence of the substrate but also allows ions to accumulate on both the top and the bottom surface of MoTe$_2$. The consequent increase of the gate capacitance resulted in an improved subthreshold swing (~73 mV/dec) and on-off ratio (10^6) at room temperature for suspended MoTe$_2$ compared to substrate-supported devices. Suspended transistors with ionic liquid gating enable larger charge density compared to ionic liquid gated supported devices, and may provide a useful platform to study screening physics in 2D materials.

Two-dimensional transition metal dichalcogenide compound (TMDC) materials have a variety of properties depending on the crystal structure and constituent elements and attract broad interests for applications in nanoelectronics and optics.[1,2] Among them, MoTe$_2$ has received increasing attention owing to its low phase transition barrier[3,4] and its sizeable bandgap close to that of Si.[5–7] MoTe$_2$ has an indirect electronic bandgap of 0.88 increasing to 1.0 eV going from bulk to few-layer, with a direct bandgap of about 1.1 eV for the monolayer.[7–11] Field-effect-transistors (FETs) based on α-MoTe$_2$ have been reported[8,12–20] and applied to logic circuits[21] and sensors.[19,22] However, much lower mobilities have been reported than the theoretically predicted phonon-limited mobility at room temperature of ~240 cm^{2}V^{-1}s^{-1} for bulk,[23] and ~100-2500 cm^{2}V^{-1}s^{-1} for monolayer,[10,24] mainly due to charged traps at the MoTe$_2$/substrate interface and Schottky barriers at the MoTe$_2$/metal contacts.[13] High-κ screening can reduce the influence of the charged traps, and an enhanced electron mobility (80 cm^{2}V^{-1}s^{-1} at room temperature) has been reported for a MoTe$_2$ device capped with Al$_2$O$_3$.[15] On the other hand, ionic liquid (IL) gating is an attractive doping method for TMDC because of the high gate capacitance of the electric double layer (EDL) formed on the sample surface. Heavy doping of the semiconductor can result in the reduction of the effective Schottky barrier, and in addition the high dielectric constant of ionic liquids can improve the performance of MoTe$_2$ FETs as shown by previous studies on substrate-supported multilayer devices.[8,25]

---

a) Electronic mail: shjhang@konkuk.ac.kr

In this letter, the electrical performance of suspended few-layer MoTe$_2$ FETs with ionic liquid gating is reported. In suspended structures, the influence of the underlying substrate is removed, and a good mobility of 90 cm^2/Vs at 360 K is achieved. In addition, the suspended structure provides another channel for IL gating to form a second EDL on the bottom surface of the MoTe$_2$, thereby further increasing the EDL capacitance. A subthreshold swing (SS) of 73 mV/dec and an on/off ratio of 10^6 at room temperature are demonstrated in a suspended device gated by an ionic liquid.

2H-type MoTe$_2$ few-layers were prepared by mechanical exfoliation on a substrate consisting of 300 nm of SiO$_2$ on highly p-doped Si. Electrodes were patterned by e-beam lithography, followed by Ti(5 nm)/Au(50 nm) or Cr(20 nm)/Au(30 nm) deposition via an e-beam evaporator. To create suspended structures, as illustrated in Fig. 1(a), PMMA was first coated on the devices and a section of PMMA was then removed by e-beam lithography. The devices were then treated with buffered oxide etchant (BOE) 6: 1 to etch the 300 nm SiO$_2$ layer. After that, MoTe$_2$ FETs were rinsed in deionized water and placed into acetone to remove residual PMMA, and finally dried in a critical point dryer (CPD). A scanning electron microscope (SEM) image of a suspended device is presented in Fig. 1(a). 9 nm-thick MoTe$_2$ with length L = 2.2 μm and width W = 3.8 μm is suspended over the trench, where all SiO$_2$ has been etched away and a 300 nm gap exists between the MoTe$_2$ and the highly p-doped Si substrate.

The suspended device was characterized in vacuum at different temperatures. Left insert of Fig. 1(b) shows the current-voltage (I_D-V_D) characteristics at a back-gate voltage V_{BG} = 0. The I_D-V_D curves are linear for $T \geq 200$ K, with a resistance of about 100 kΩ at T = 360 K. The transfer curves of the device at V_D = 0.1 V are displayed in Fig. 1(b). The field-effect mobility for electrons μ_e is estimated from the maximum transconductance with a gate capacitance of ~ 4 nF/cm^2 (see Supplementary Information). μ_e of ~90 and ~80 cm^2/Vs are obtained at 360 and 260 K, respectively, much higher than values (0. 1 – 40 cm^2/Vs) reported for conventional MoTe$_2$ FETs at room temperature[12–16] and comparable to 80 cm^{2}V^{-1}s^{-1} reported for a device capped with Al$_2$O$_3$.[15] This enhancement in the electron mobility is due to the device being suspended. In the suspended structure, unlike supported devices, the MoTe$_2$ channel can avoid charge traps at the substrate interface and be free from the influence of the substrate roughness and surface polar optical phonon scattering. On the other hand, notice that V_{BG} is applied for a narrow range of -15 to +15 V to restrict the capacitive force between the MoTe$_2$ and the gate to ~100 nN (see Supplementary Information for calculation). Upon applying a larger V_{BG} to other suspended devices, the transfer curves were found to differ in repeated gate-sweeps and the MoTe$_2$ eventually collapsed to the Si surface. The low Young's modulus of MoTe$_2$, 110 GPa,[26,27] which is about ten times lower than ~1 TPa of carbon nanotubes[28] or graphene,[29] and the relatively long strain relaxation time (~minutes)[30] originating from the structural phase transition between the 1T` and 2H phases leave the suspended MoTe$_2$ FETs vulnerable to

the capacitive force between the $MoTe_2$ and the gate. With the low dielectric constant of vacuum (~1/4 of that of SiO_2), the gate capacitance of the suspended device is one-third of that of a device supported on 300 nm SiO_2. The gate range applied above corresponds to a mere -5 to +5 V back-gate for a 300 nm-SiO_2 supported device, and the ambipolar behavior of $MoTe_2$ FETs[16–21] cannot be seen in Fig. 1(b). The right inset of Fig. 1(b) shows the transfer curves in a log scale. While the device at 360 K is not completely turned off in the narrow gate range, an on/off ratio of 10^7 is observed at $T = 77$ K with a subthreshold swing of 0.9 V/dec. Also, we note the extracted mobility increases with temperature, in contrast to reports on supported devices that have shown a decreasing mobility from 200 to 353 K for oxide-encapsulated devices[31] or decreasing mobility from 77 to 180 K for an IL-gated supported device.[32] The temperature dependence of the mobility often depends on V_D for FETs based on TMDCs because of the Schottky barrier formed at the interface between the TMDC and the metal electrodes.[33] The observed positive T-dependence of mobility indicates the dominant role of the Schottky barrier at low temperatures and low drain bias.[33] The contact resistance R_c, estimated by the Y function method (see Supplementary Information), is ~52 kΩμm at 360 K, which is about 1/5 of the total device resistance, and R_c increases to ~530 kΩμm at 200 K, resulting in the positive T-dependence of the mobility. At low drain bias, the field-effect mobility can be underestimated due to the contact resistance. Intrinsic mobility, extracted from the Y function method, is estimated to be ~110 cm^2/Vs at 360 K (see Supplementary Information), larger than ~90 cm^2/Vs including contact resistance. The activation energy can be extracted by fitting the conductance G with the expression $G(T) = G_0 \exp(-E_a/k_B T)$, where G_0 is a fitting parameter with k_B being Boltzmann's constant. The Arrhenius plot is shown in the inset of Fig. 1(c), and the extracted activation energy is displayed in Fig. 1(c). The activation energy decreased from 66 to 15 meV as the gate voltage increased from -15 to +15 V. Since $E_a = E_C - E_F$, with E_C being the conduction band minimum, this indicates the Fermi level E_F is located close to the conduction band edge, and E_a decreases with V_{BG} as the Fermi level further approaches the conduction band. However, E_a is flattened for $V_{BG} > -5$ V, which can be related to the presence of the Schottky barrier. The activation energy of ~ 30 meV seen at $V_{BG} = -5$ V is comparable to the Schottky barrier height of ~40 meV, reported for a $Ti/MoTe_2$ junction.[34] On the other hand, as pointed out by Mleczko $et\ al.$[20], the Arrhenius analysis may underestimate the barrier height by interpreting the tunneling contribution as thermionic current.

We now turn our attention to ionic liquid gating of suspended $MoTe_2$ FETs. The high dielectric constant of the ionic liquid and its encirclement of $MoTe_2$ significantly lower the vulnerability of the suspended device to the capacitive force. In addition, the suspended structure allows ions to accumulate on both the top and the bottom surface of $MoTe_2$, thereby enabling a higher gate capacitance. N,N-Diethyl-N-methyl-N-(2-methoxyethyl)ammonium bis(trifluoromethylsulfonyl)imide ([DEME][TFSI]), with a dielectric constant $\kappa \sim 15$,[35] was used for ionic liquid gating. DEME acts as the cation and TFSI acts as the anion. Ionic

3

liquids have hygroscopicity and moisture penetrates easily. Moisture penetration lowers the charge density of the ionic liquid.[36,37] To minimize this effect, the device was heated at 100°C in low vacuum for several hours before the electrical properties were measured. To make a direct comparison between suspended and substrate-supported MoTe$_2$ transistors when gated by the ionic liquid, multiple Cr/Au electrodes were deposited on a large 6 nm-thick MoTe$_2$ sample with $W = 1$ μm. As shown in Fig. 2(a), a supported and a suspended device are created on a single MoTe$_2$ crystal. An SEM image of the suspended part is presented in the lower part of Fig. 2(a).

Prior to the application of the ionic liquid, the transfer characteristics of back gated MoTe$_2$ was compared for the suspended and the supported devices (Fig. 2(b)). The device supported on the SiO$_2$ substrate exhibits n-type behaviour with an on/off ratio of 10^4 and a subthreshold swing of 6.0 V/dec, when measured with $|V_{BG}| \leq 60$ V at room temperature in vacuum, while the suspended device remains turned on. Recall that the gate efficiency of the suspended device is one-third of that of the supported device due to the low dielectric constant of vacuum. The field-effect mobility for electrons is estimated to be ~0.8 cm^2/Vs for the supported and ~4 cm^2/Vs for the suspended transistor. The removal of the underlying substrate resulted in a five times enhancement of mobility.

 [DEME] [TFSI] was dropped on the devices and the transfer characteristics were investigated again (Fig. 2(c)). Upon the application of IL gating using a side electrode, ambipolar behavior, absent when back gated, was clearly observed for both devices. The on/off ratio was improved to 10^5 for the supported and 10^6 for the suspended transistor. The subthreshold swing was extracted from the slope $|\partial \log (I_D)/\partial V_{BG}|_{max}$ for both the electron SS_e and hole side SS_h. As for the supported device, SS_e is greatly improved from 6.0 V/dec (back-gating) to ~250 mV/dec (IL-gating), and SS_h is evaluated to be ~ 310 mV/dec. Interestingly, an even lower subthreshold swing is observed in the suspended device, with SS_e ~ 73 mV/dec and SS_h ~ 120 mV/dec. SS_e persists between 7×10^{-5} and 7×10^{-2} μA/μm, over three decades. Reduced subthreshold swings and ambipolar characteristics are explained by the high coupling efficiency of the IL gate, as has been reported for many ion-gated TMDC FETs.[8,25,32,38] A layer of cations or anions accumulates on the MoTe$_2$ surface and forms an electric double layer as illustrated in the inset of Fig. 2(c), resulting in a greater capacitance compared with the back-gate geometry. In addition, in the suspended device, ions can accumulate on both sides (top and bottom) of MoTe$_2$, and the further enhanced EDL capacitance accounts for a smaller SS and a larger on/off ratio in the suspended than in the supported device. The value of SS_e ~ 73 mV/dec, observed with the suspended device, is also lower than SS_e~140 mV/dec reported elsewhere for a supported MoTe$_2$ gated by the same IL,[8] or SS_e~100 mV/dec for a supported MoTe$_2$ FET using poly(ethylene oxide)-CsClO$_4$ electrolyte.[25] Note the SS of the

4

suspended $MoTe_2$ FET is close to the thermionic limit of SS (~60 mV/dec). By adopting EDL capacitances, 7.2 $\mu F/cm^2$ for electrons, 4.7 $\mu F/cm^2$ for holes,[39] determined from an experiment with a [DEME] [TFSI] gate, the electron and hole mobilities were estimated to be $\mu_e \approx 3$ cm^2/Vs and $\mu_h \approx 4$ cm^2/Vs, respectively, for the supported device. The mobility increases by about a factor of four from ~0.8 cm^2/Vs after the application of IL. For the suspended device, the same estimation gives $\mu_e \approx 16$ cm^2/Vs and $\mu_h \approx 26$ cm^2/Vs. However, the access of ions to both surfaces of $MoTe_2$ may increase the EDL capacitance. Although the underside gating may not be equivalent to the top, the simple assumption that the EDL capacitance increases by a factor of two in the suspended structure suggests $\mu_e \approx 8$ cm^2/Vs and $\mu_h \approx 13$ cm^2/Vs. The mobility of the suspended $MoTe_2$ also increased with the presence of IL and remained superior to that of the supported device. Enhanced mobility after the application of IL, observed for both the supported and suspended devices, can be attributed to the reduced scattering from charged impurities by the high-κ ionic liquid.

Finally, Figure 3 shows the results of an investigation of the ambient air stability of IL-gated $MoTe_2$ FETs. For comparison, transfer curves of a conventional back-gated $MoTe_2$ transistor were recorded over 11 days and displayed in Fig. 3(a). It can be clearly seen in the transfer curves in a log scale (inset of Fig.3 (a)) that the charge neutrality points gradually moved to the right, as $MoTe_2$ reacted with oxygen over time. The electron mobility also decreased from 0.5 to 0.2 cm^2/Vs. This observation is consistent with previous studies on the oxygen interaction with $MoTe_2$ FETs.[19,40] In Fig. 3(b), the transfer curves of a IL-gated device recorded over 27 days are shown. By covering with the ionic liquid, the $MoTe_2$ avoided direct contact with air and the charge neutrality point remained stable over the whole period. On the other hand, the on-current of the device decreased with time, which consequently reduced the on/off ratio over the period. Ionic liquids are hygroscopic, and water slowly accumulates in the IL to a saturation level corresponding to the humidity. Moisture lowers the charge density of the IL, leading to the decreased on-current. For another IL-gated $MoTe_2$, kept in vacuum, the electrical performance of the device remained almost the same after 30 days (see Supplementary Information).

In summary, the performance and the IL gating of suspended $MoTe_2$ FETs has been investigated. Free from the influence of the substrate, the mobility of suspended few-layer $MoTe_2$ reached 90 cm^2/Vs at 360 K. However, the suspended $MoTe_2$ FETs are vulnerable to the capacitive force between the $MoTe_2$ and the back gate due to the relatively low Young's modulus of $MoTe_2$ and the relatively long strain relaxation time. Turning to the ionic liquid gating of suspended $MoTe_2$, we find the high dielectric constant of IL and its encirclement of $MoTe_2$ significantly lower the vulnerability to the capacitive force. In addition, the suspended structure allows ions to accumulate on both the top and the bottom surface of $MoTe_2$, resulting in a larger EDL capacitance. We report an electron subthreshold swing of ~73 mV/dec, the lowest in $MoTe_2$ FET reported so far, with an on-

off ratio of 10^6 for the suspended $MoTe_2$. Application of IL gating to suspended 2D materials provides a way to a larger charge induction and can be a useful platform to study 2D screening properties.

See the supplementary information for the estimation of gate capacitance, capacitive force, low-field mobility and contact resistance.

AUTHOR`S CONTRIBUTIONS

W.R.Choi and J.H.Hong contributed equally to this work.

DATA AVAILABILITY

The data that supports the findings of this study are available within the article and its supplementary material.

REFERENCES

[1] S. Manzeli, D. Ovchinnikov, D. Pasquier, O. V. Yazyev, and A. Kis, Nat. Rev. Mater. **2**, 17033 (2017).

[2] Y. Liu, N.O. Weiss, X. Duan, H.-C. Cheng, Y. Huang, and X. Duan, Nat. Rev. Mater. **1**, 16042 (2016).

[3] W. Hou, A. Azizimanesh, A. Sewaket, T. Peña, C. Watson, M. Liu, H. Askari, and S.M. Wu, Nat. Nanotechnol. **14**, 668 (2019).

[4] K.-A.N. Duerloo, Y. Li, and E.J. Reed, Nat. Commun. **5**, 4214 (2014).

[5] D. Yang, X. Hu, M. Zhuang, Y. Ding, S. Zhou, A. Li, Y. Yu, H. Li, Z. Luo, L. Gan, and T. Zhai, Adv. Funct. Mater. **28**, 1800785 (2018).

[6] Y. Xie, E. Wu, J. Zhang, X. Hu, D. Zhang, and J. Liu, ACS Appl. Mater. Interfaces **11**, 14215 (2019).

[7] J. Kang, S. Tongay, J. Zhou, J. Li, and J. Wu, Appl. Phys. Lett. **102**, 012111 (2013).

[8] I.G. Lezama, A. Ubaldini, M. Longobardi, E. Giannini, C. Renner, A.B. Kuzmenko, and A.F. Morpurgo, 2D Mater. **1**, 021002 (2014).

[9] I.G. Lezama, A. Arora, A. Ubaldini, C. Barreteau, E. Giannini, M. Potemski, and A.F. Morpurgo, Nano Lett. **15**, 2336 (2015).

[10] A. Rawat, N. Jena, D. Dimple, and A. De Sarkar, J. Mater. Chem. A **6**, 8693 (2018).

[11] H.G. Kim and H.J. Choi, Phys. Rev. B **103**, 1 (2021).

[12] S. Cho, S. Kim, J.H. Kim, J. Zhao, J. Seok, D.H. Keum, J. Baik, D.-H. Choe, K.J. Chang, K. Suenaga, S.W. Kim, Y.H. Lee, and H. Yang, Science **349**, 625 (2015).

6

[13] H. Ji, G. Lee, M.-K. Joo, Y. Yun, H. Yi, J.-H. Park, D. Suh, and S.C. Lim, Appl. Phys. Lett. **110**, 183501 (2017).

[14] J.H. Sung, H. Heo, S. Si, Y.H. Kim, H.R. Noh, K. Song, J. Kim, C.-S. Lee, S.-Y. Seo, D.-H. Kim, H.K. Kim, H.W. Yeom, T.-H. Kim, S.-Y. Choi, J.S. Kim, and M.-H. Jo, Nat. Nanotechnol. **12**, 1064 (2017).

[15] D. Qu, X. Liu, M. Huang, C. Lee, F. Ahmed, H. Kim, R.S. Ruoff, J. Hone, and W.J. Yoo, Adv. Mater. **29**, 1606433 (2017).

[16] W. Luo, M. Zhu, G. Peng, X. Zheng, F. Miao, S. Bai, X.-A. Zhang, and S. Qin, Adv. Funct. Mater. **28**, 1704539 (2018).

[17] T. Liu, D. Xiang, Y. Zheng, Y. Wang, X. Wang, L. Wang, J. He, L. Liu, and W. Chen, Adv. Mater. **30**, 1804470 (2018).

[18] S. Nakaharai, M. Yamamoto, K. Ueno, Y.-F. Lin, S.-L. Li, and K. Tsukagoshi, ACS Nano **9**, 5976 (2015).

[19] S.-H. Yang, C.-Y. Lin, Y.-M. Chang, M. Li, K.-C. Lee, C.-F. Chen, F.-S. Yang, C.-H. Lien, K. Ueno, K. Watanabe, T. Taniguchi, K. Tsukagoshi, and Y.-F. Lin, ACS Appl. Mater. Interfaces **11**, 47047 (2019).

[20] M.J. Mleczko, A.C. Yu, C.M. Smyth, V. Chen, Y.C. Shin, S. Chatterjee, Y.-C. Tsai, Y. Nishi, R.M. Wallace, and E. Pop, Nano Lett. **19**, 6352 (2019).

[21] Y.-F. Lin, Y. Xu, S.-T. Wang, S.-L. Li, M. Yamamoto, A. Aparecido-Ferreira, W. Li, H. Sun, S. Nakaharai, W.-B. Jian, K. Ueno, and K. Tsukagoshi, Adv. Mater. **26**, 3263 (2014).

[22] Z. Feng, Y. Xie, J. Chen, Y. Yu, S. Zheng, R. Zhang, Q. Li, X. Chen, C. Sun, H. Zhang, W. Pang, J. Liu, and D. Zhang, 2D Mater. **4**, 025018 (2017).

[23] A. Conan, A. Bonnet, M. Zoaeter, and D. Ramoul, Phys. Status Solidi **124**, 403 (1984).

[24] W. Zhang, Z. Huang, W. Zhang, and Y. Li, Nano Res. **7**, 1731 (2014).

[25] H. Xu, S. Fathipour, E.W. Kinder, A.C. Seabaugh, and S.K. Fullerton-Shirey, ACS Nano **9**, 4900 (2015).

[26] P. May, U. Khan, and J.N. Coleman, Appl. Phys. Lett. **103**, 163106 (2013).

[27] M.L. Pereira Júnior, C.M. Viana de Araújo, J.M. De Sousa, R.T. de Sousa Júnior, L.F. Roncaratti Júnior, W. Ferreira Giozza, and L.A. Ribeiro Júnior, Condens. Matter **5**, 73 (2020).

[28] N. Yao and V. Lordi, J. Appl. Phys. **84**, 1939 (1998).

[29] J.U. Lee, D. Yoon, and H. Cheong, Nano Lett. **12**, 4444 (2012).

[30] S. Song, D.H. Keum, S. Cho, D. Perello, Y. Kim, and Y.H. Lee, Nano Lett. **16**, 188 (2016).

[31] J.Y. Shang, M.J. Moody, J. Chen, S. Krylyuk, A. V. Davydov, T.J. Marks, and L.J. Lauhon, ACS Appl. Electron. Mater. **2**, 1273 (2020).

[32] M.M. Perera, M.-W. Lin, H.-J. Chuang, B.P. Chamlagain, C. Wang, X. Tan, M.M.-C. Cheng, D. Tománek, and Z. Zhou, ACS Nano **7**, 4449 (2013).

[33] X. Liu, J. Hu, C. Yue, N. Della Fera, Y. Ling, Z. Mao, and J. Wei, ACS Nano **8**, 10396 (2014).

[34] N.J. Townsend, I. Amit, M.F. Craciun, and S. Russo, 2D Mater. **5**, 025023 (2018).

[35] F. Wang, P. Stepanov, M. Gray, C.N. Lau, M.E. Itkis, and R.C. Haddon, Nano Lett. **15**, 5284 (2015).

[36] A. Maiti, A. Kumar, and R.D. Rogers, Phys. Chem. Chem. Phys. **14**, 5139 (2012).

[37] S. Cuadrado-Prado, M. Domínguez-Pérez, E. Rilo, S. García-Garabal, L. Segade, C. Franjo, and O. Cabeza, Fluid Phase Equilib. **278**, 36 (2009).

[38] S. Jo, N. Ubrig, H. Berger, A.B. Kuzmenko, and A.F. Morpurgo, Nano Lett. **14**, 2019 (2014).

[39] Y. Zhang, J. Ye, Y. Matsuhashi, and Y. Iwasa, Nano Lett. **12**, 1136 (2012).

[40] S.P. Wang, R.J. Zhang, L. Zhang, L.F. Feng, and J. Liu, J. Mater. Sci. **54**, 3222 (2019).
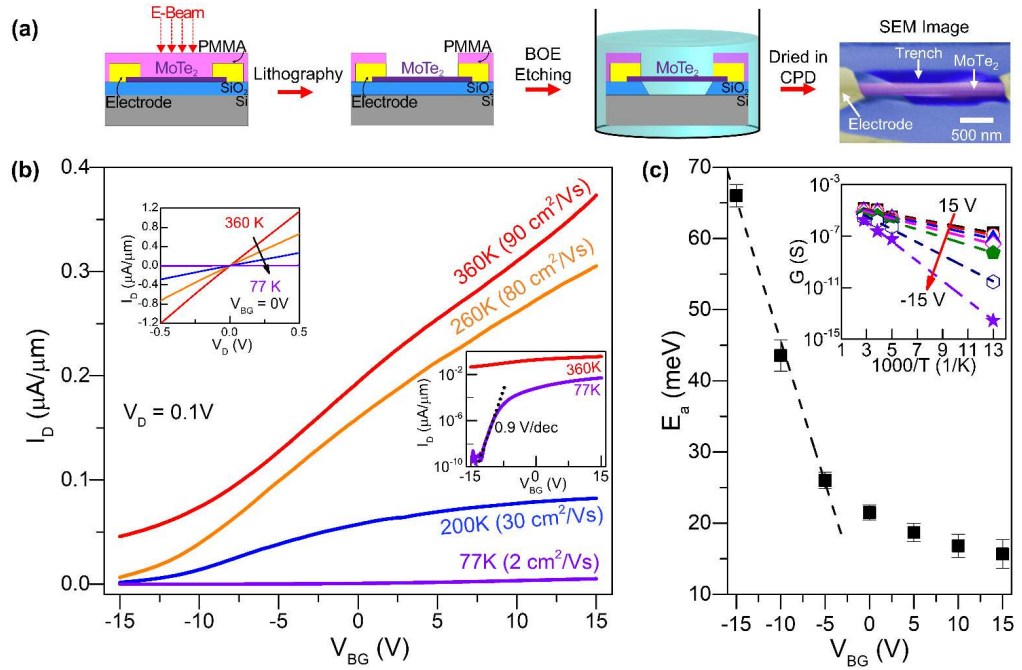
FIG. 1. (a) Fabrication procedure of a suspended MoTe$_2$ device and a false colored SEM image of resulting suspended MoTe$_2$ device. **(b)** Drain current per unit width versus gate voltage for the suspended MoTe$_2$ device at different temperatures. (Left Inset: drain-source current-voltage characteristics at V_{BG} = 0 V, Right Inset: Transfer curves in a log scale for 77 and 360 K) **(c)** Thermal activation energy as a function of gate-voltage, extracted from the Arrhenius plots of conductance (inset). E_a is flattened for V_{BG} > -5 V (see dashed line), possibly indicating the role of a Schottky barrier formed at MoTe$_2$/Ti electrodes.
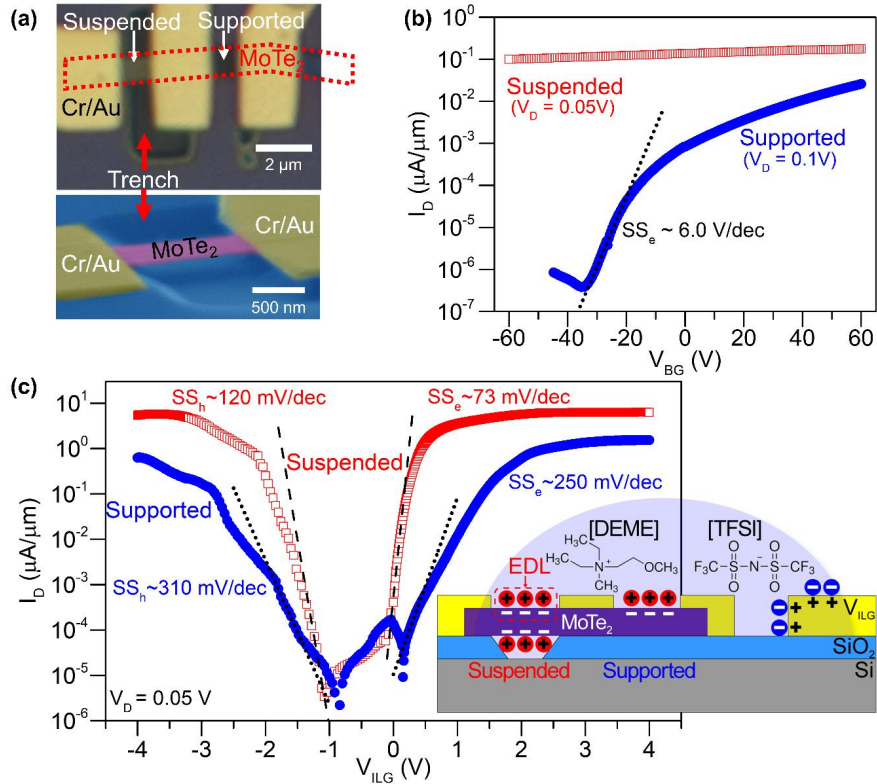
9

FIG. 2. (a) An optical image of supported and suspended devices created with a 6 nm-thick MoTe$_2$ crystal. To make a direct comparison between the suspended and the substrate-supported FETs, multiple Cr/Au electrodes were deposited on a large MoTe$_2$ sample. Lower figure shows a zoomed-in SEM image of the suspended part. Note the width of trench (~6 μm) is much wider than the width of MoTe$_2$ (~1 μm) ensuring EDL formation underneath the surface of MoTe$_2$. **(b)** Transfer characteristics of the suspended (hollow red square) and the supported (filled blue dot) MoTe$_2$ FETs with Si back gate at room temperature. **(c)** Transfer characteristics of the suspended (hollow red square) and the supported (filled blue dot) MoTe$_2$ devices with ionic liquid gate V_{ILG} at room temperature. Inset shows a schematic illustration of the application of ionic liquid gate to MoTe$_2$ FETs and explains the electric double layer (EDL) formed on the surface of MoTe$_2$.

(a)

MoTe$_2$ back-gated

0 day

2

4

8

11

I_D (nA/µm)

V_{BG} (V)

V_D = 0.1 V

Inset: I_D (µA/µm) vs V_{BG} (V), 0 day, 11 days

(b)

MoTe$_2$ IL-gated

0 day

15

16

25

27

I_D (nA/µm)

V_{ILG} (V)

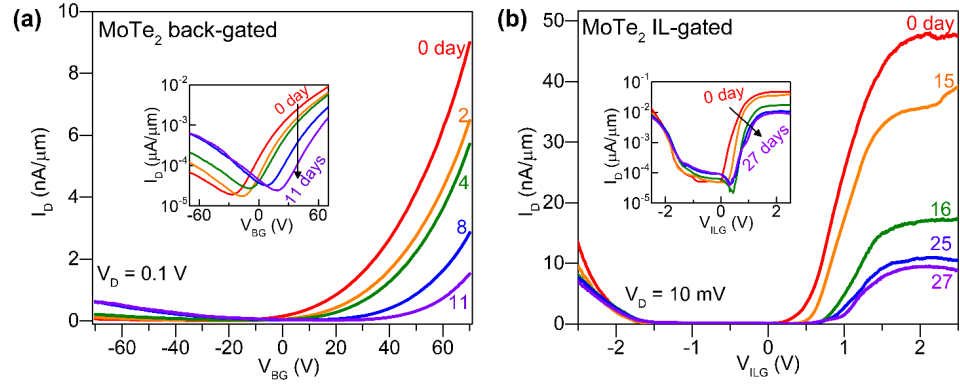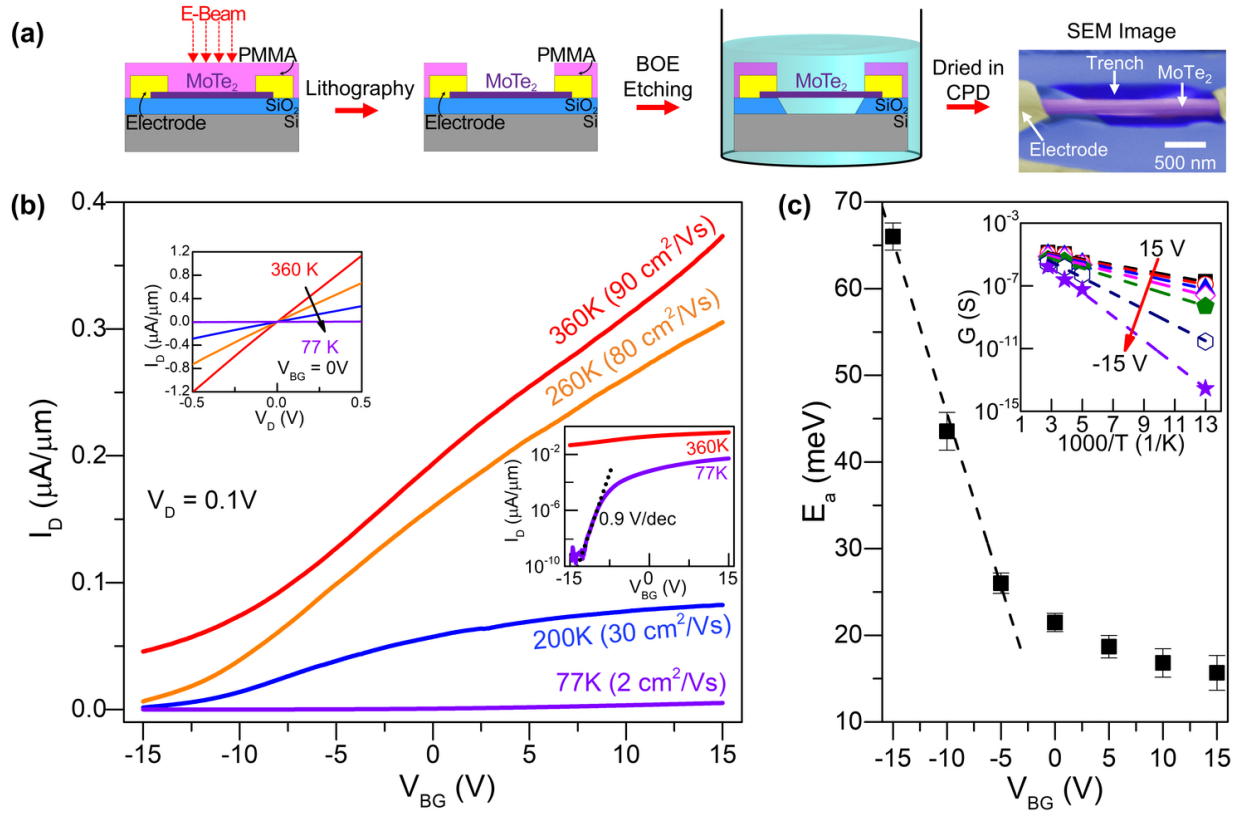V_D = 10 mV

Inset: I_D (µA/µm) vs V_{ILG} (V), 0 day, 27 days

FIG. 3. (a) Transfer curves of a conventional back-gated MoTe$_2$ transistor ($L = 2$ µm, $W = 4.5$ µm, and the thickness of 14 nm) recorded over 11 days. (Inset: log scale graph) **(b)** Transfer curves of an IL-gated device ($L = 5$ µm, $W = 15.5$ µm, and the thickness of 12 nm) studied for 27 days (Inset: log scale graph)
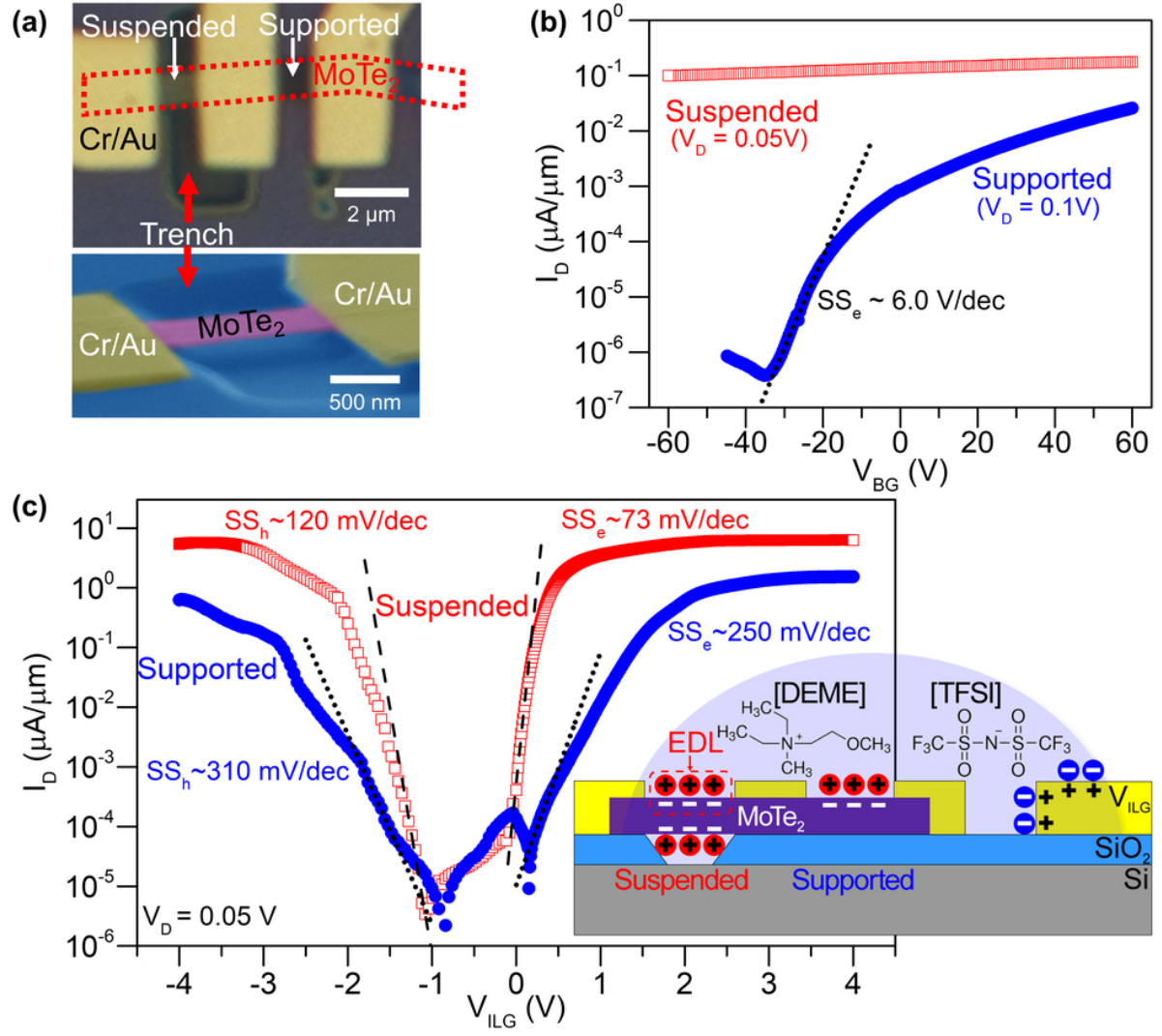
11

(a) E-Beam, PMMA, MoTe₂, SiO₂, Electrode, Si → Lithography → PMMA, MoTe₂, SiO₂, Electrode, Si → BOE Etching → MoTe₂, SiO₂, Si → Dried in CPD → SEM Image: Trench, MoTe₂, Electrode, 500 nm

(b) I_D (μA/μm) vs V_{BG} (V); $V_D = 0.1$V; 360K (90 cm²/Vs), 260K (80 cm²/Vs), 200K (30 cm²/Vs), 77K (2 cm²/Vs). Inset top: I_D (μA/μm) vs V_D (V), 360 K, 77 K, $V_{BG} = 0$V. Inset bottom: I_D (μA/μm) vs V_{BG}^0 (V), 360K, 77K, 0.9 V/dec.

(c) E_a (meV) vs V_{BG} (V). Inset: G (S) vs 1000/T (1/K), 15 V, -15 V.

(a) Suspended   Supported
MoTe$_2$
Cr/Au
2 µm
Trench
Cr/Au   MoTe$_2$ Cr/Au
500 nm

(b)
I_D (µA/µm)
Suspended
(V_D = 0.05V)
Supported
(V_D = 0.1V)
SS$_e$ ~ 6.0 V/dec
V_{BG} (V)

(c)
I_D (µA/µm)
SS$_h$~120 mV/dec   SS$_e$~73 mV/dec
Suspended
Supported
SS$_e$~250 mV/dec
SS$_h$~310 mV/dec
V_D = 0.05 V
V_{ILG} (V)
[DEME]   [TFSI]
EDL   H$_3$C—N$^+$—OCH$_3$ F$_3$C—S—N$^-$—S—CF$_3$
CH$_3$
MoTe$_2$ V_{ILG}
SiO$_2$
Suspended   Supported   Si